Mechanistic origin and preimplantation development of uniparental and polyploid blastomeres

Yan Zhao[1,6,7], Andrea Fernández-Montoro[2,7], Greet Peeters[1], Tatjana Jatsenko[1], Tine De Coster[2], Daniel Angel-Velez[2,3], Thomas Lefevre[4], Thierry Voet[4,5], Olga Tšuiko[1], Ants Kurg[6], Katrien Smits[2], Ann Van Soom[2], Joris Robert Vermeesch[1]

[1]Laboratory for Cytogenetics and Genome Research, Department of Human Genetics, KU Leuven, 3000 Leuven, Belgium

[2]Department of Internal Medicine, Reproduction, and Population Medicine - Ghent University, 9820, Merelbeke, Belgium.

[3]Research Group in Animal Sciences – INCA-CES, Universidad CES, 050021 Medellin, Colombia

[4]Laboratory of Reproductive Genomics, Department of Human Genetics, KU Leuven, 3000 Leuven, Belgium

[5]KU Leuven Institute for Single Cell Omics (LISCO), University of Leuven, KU Leuven, Leuven, Belgium

[6]Department of Biotechnology, Institute of Molecular and Cell Biology, University of Tartu, 51010, Tartu, Estonia

[7]These authors contributed equally

Corresponding author: Joris.Vermeesch@KULeuven.be

Abstract

Whole-genome (WG) abnormalities, such as uniparental diploidy and triploidy, cause fetal death. Occasionally, they coexist with biparental diploid cells in live births. Understanding the origin and early development of WG abnormal blastomeres is crucial for explaining the formation of androgenotes, gynogenotes, triploidy, chimerism, and mixoploidy. By haplotyping 118 blastomeres from first cleavages, we identified various mechanisms of heterogoneic divisions that lead to WG abnormal blastomeres or their coexistence with normal blastomeres in both multipolar and bipolar cleaving zygotes. After culturing the totipotent blastomeres to three preimplantation stages and performing transcriptome profiling on over 600 cells, we discovered that stress responses contribute to developmental impairment in WG abnormal cells, resulting in either cell arrest or blastocyst formation. However, first-cleavage-derived WG abnormal blastomeres can survive early development and progress to blastocysts. Their potential dominance in preimplantation embryos represents an overlooked cause of abnormal development. Haplotype based screening could further increase pregnancy rates.

Introduction

Chromosomal abnormalities are common during human development, especially in the preimplantation phase(Hassold and Hunt 2001; Vanneste et al. 2009; Hassold et al. 1980). One notable category of chromosome abnormalities are whole-genome (WG) anomalies(Masset et al. 2021). Embryos bearing WG abnormalities contain abnormal

levels of parental genomes rather than the normal diploid constellation with one maternal and one paternal haploid genome. For instance, uniparental haploid or diploid embryos carry only chromosomes from a single parent, while triploid embryos contain an additional haploid set of chromosomes from one of the parents. Constitutional WG anomalies are generally lethal during the embryonic stage. Triploidy occurs in approximately 1% of all conceptuses, contributing to around 10% of all spontaneous abortions(Zaragoza et al. 2000; Hassold et al. 1980) with extremely rare live born cases surviving less than a year(Sherard et al. 1986). Complete and partial hydatidiform moles, occurring at rates of 1 in 1000 and 3 in 1000 pregnancies respectively, are primarily androgenetic diploid and diandric triploid, respectively(Seckl et al. 2010). Mosaic forms with coexistence of normal cells can result in rare cases of live birth. For example, gynogenetic and androgenetic chimerism (coexistence of uniparental and normal cells) and diploid/triploid mixoploidy (coexistence of triploid and normal cells) have been reported in live-born individuals with congenital abnormalities(Madan 2020). As a model organism with a developmental process and an aneuploidy profile similar to that of humans(Tšuiko et al. 2017; Hansen 2010; Santos et al. 2014), WG abnormalities have also been identified at various stages during bovine development(Dunn et al. 1970; Tšuiko et al. 2017; Destouni et al. 2016; Meinecke et al. 2003; De Coster et al. 2022).

Several models have been proposed to explain the mechanistic origins of WG abnormalities in embryos(Masset et al. 2021). These include dispermy or diploid oocytes leading to triploidy, as well as parthenogenetic division of the oocyte or

fertilization of an 'empty' egg resulting in uniparental embryos. While these models explain the origin of triploid or uniparental embryos, they are limited by the deduction from surviving cells at later developmental stages. Additionally, the mechanistic origins of chimerism and mixoploidy remain speculative(Madan 2020; Masset et al. 2021). Since all body cells stem from a single zygote, diverse WG abnormalities observed during the late developmental stages are likely the result of irregular zygotic cleavages. Our recent study with bovine *in vitro* fertilized embryos provides direct evidence of a non-canonical first zygotic division as the mechanistic origin of cell lines exhibiting WG abnormalities(De Coster et al. 2022), which we termed "heterogoneic division". This specialized division involves the segregation of entire parental genomes into distinct blastomeres, often triggered by polyspermy and occurring concurrently with multipolar zygotic division. Embryos following heterogoneic division typically contain blastomeres with diverse chromosomal constitutions, including biparental diploid, polyploid, and uniparental blastomeres, resembling those identified in chimeric and mixoploid individuals. Such cleavage involving WG segregation errors has also been reported in *in vitro* human and non-human primate embryos(Daughtry et al. 2019; Ottolini et al. 2017).

Heterogoneic division, as the natural origin of blastomeres with WG abnormalities, represents a fundamental yet underexplored aspect of embryo development. While research on preimplantation embryo development often focuses on aneuploidies and their implications(Fragouli et al. 2013; Fernandez Gallardo et al. 2023; Tšuiko et al. 2021), there has been a lack of investigation into the developmental trajectory of

spontaneously arising blastomeres carrying WG abnormalities. Examining the subsequent development of blastomeres following both heterogoneic and normal first zygotic divisions will provide valuable insights into the developmental disparities between blastomeres with WG abnormalities and normal blastomeres. Such insights are essential for advancing our understanding of the mechanistic origins of triploidy, moles, chimerism, and mixoploidy identified late during development, and will guide genetic testing and embryo selection strategies regarding WG abnormalities.

Here, we explored the genome constitution and developmental potential of individual blastomeres resulting from both bi- and multipolar first zygotic divisions. Through haplotyping of 118 blastomere outgrowths collected at three preimplantation stages, we demonstrated that uniparental and polyploid blastomeres arise from both multipolar and bipolar cleaving zygotes and exhibit a reduced blastocyst rate. Along with single-cell transcriptome analysis of 446 transcriptomes from 124 blastomere outgrowths, we observed impaired transcriptomic development in blastomere outgrowths carrying WG abnormalities, starting from major embryonic genome activation (EGA). This impaired development is attributed to stress responses induced in blastomere outgrowths with WG abnormalities during EGA. Despite these challenges, some blastomere outgrowths with WG abnormalities successfully managed this stress period and progressed to the blastocyst stage, underscoring their potential significant role in abnormal embryo development.

Results

Whole-genome segregation errors occur in multipolar and bipolar first cleavages

To investigate the developmental program of gynogenetic/androgenetic and polyploid blastomeres following spontaneous heterogoneic division, we exploited the totipotency of blastomeres from early cleavage-stage embryos(Johnson et al. 1995; Willadsen 1980). Daughter blastomeres from 17 bipolar and 35 multipolar cleaved embryos were dissected and individually cultured to either day 2 (T1, 72 hours post fertilization (hpf), 4-6 cell stage), day 4 (T2, 121 hpf, 4-12 cell stage), or day 6 (T3, 170 hpf, blastocyst stage) post blastomere splitting, respectively (**Fig. 1**).

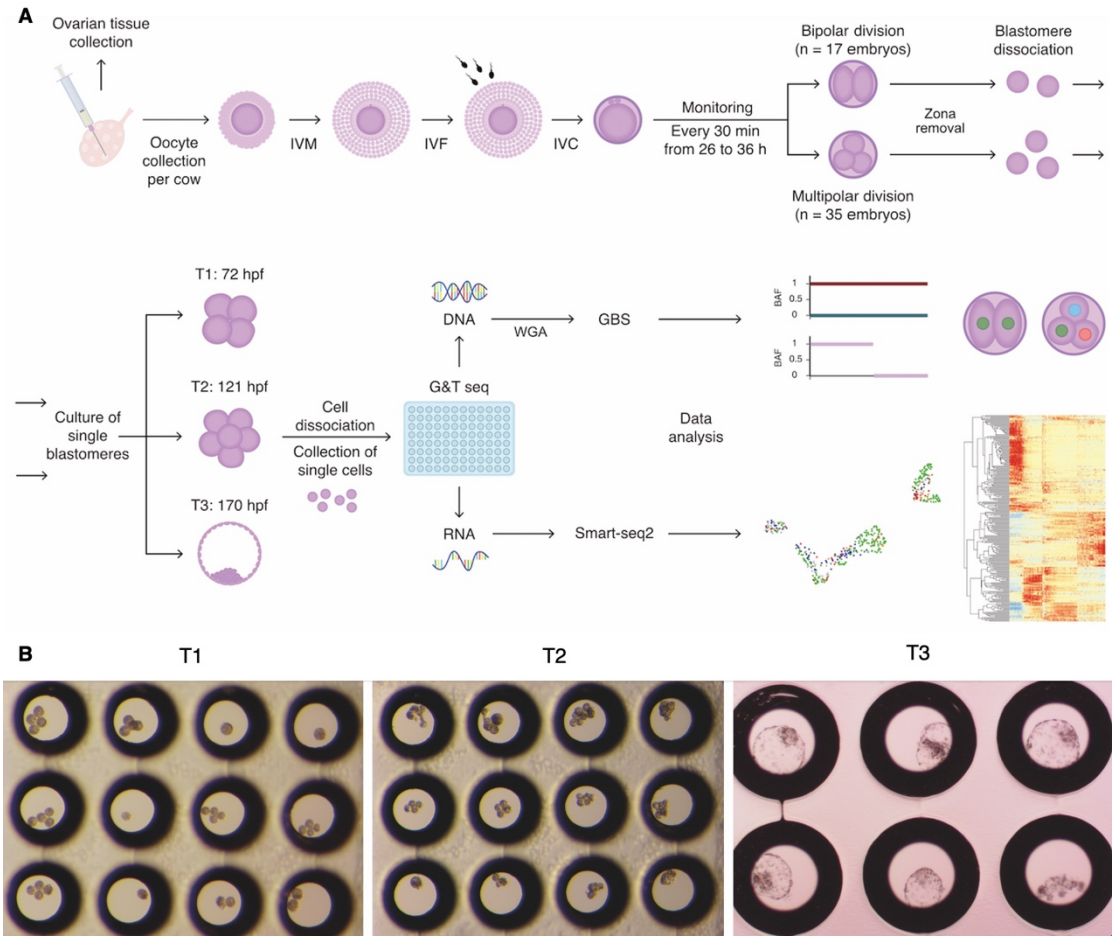

Figure 1. Experimental setup. (A) Diagram illustrating the experimental design. Bovine embryos were created and cultured *in vitro*. After the first zygotic division, blastomeres were

dissected and cultured to three preimplantation timepoints. Blastomere outgrowths were subsequently collected and dissected into single cells. Each dissected cell underwent genome and transcriptome separation followed by sequencing. Genome data were used for haplotyping and copy number profiling, while transcriptome data were used for gene expression analysis. Genome and transcriptome sequencing (G&T-seq): Protocol for isolating poly(A) RNA and genomic DNA from single cells. Genotyping-by-sequencing (GBS): Sequencing-based protocol for genome-wide haplotyping and copy number profiling. (B) Example images of blastomere outgrowths collected at T1, T2, and T3, respectively.

To determine the chromosomal constitution of the blastomeres in culture, we performed genome-wide haplotyping and copy number profiling on cells derived from blastomere outgrowths using genotyping-by-sequencing (GBS) (Masset et al. 2022) (**Fig. 1**). We successfully inferred the chromosomal constitution for all cultured blastomeres in 31 embryos and a subset of cultured blastomeres in 12 embryos, totally getting the chromosomal constitution of 118 blastomeres in culture (**Fig. 2A,B; Supplemental Tables S1,S2**). Among these, 45% (n=53) were identified as biparental diploid, while 41% (n=48) exhibited WG abnormalities, including 35 androgenetic, 9 gynogenetic, 3 diandric triploid, and 1 triandric tetraploid blastomeres. Additionally, 14% (n=17) of the blastomeres in culture with inferred chromosomal constitution were found to be anuclear. All anuclear blastomeres and the majority (96%, 46 out of 48) of blastomeres with WG abnormalities originated from embryos undergoing multipolar first cleavage (**Fig. 2B; Supplemental Table S1**).

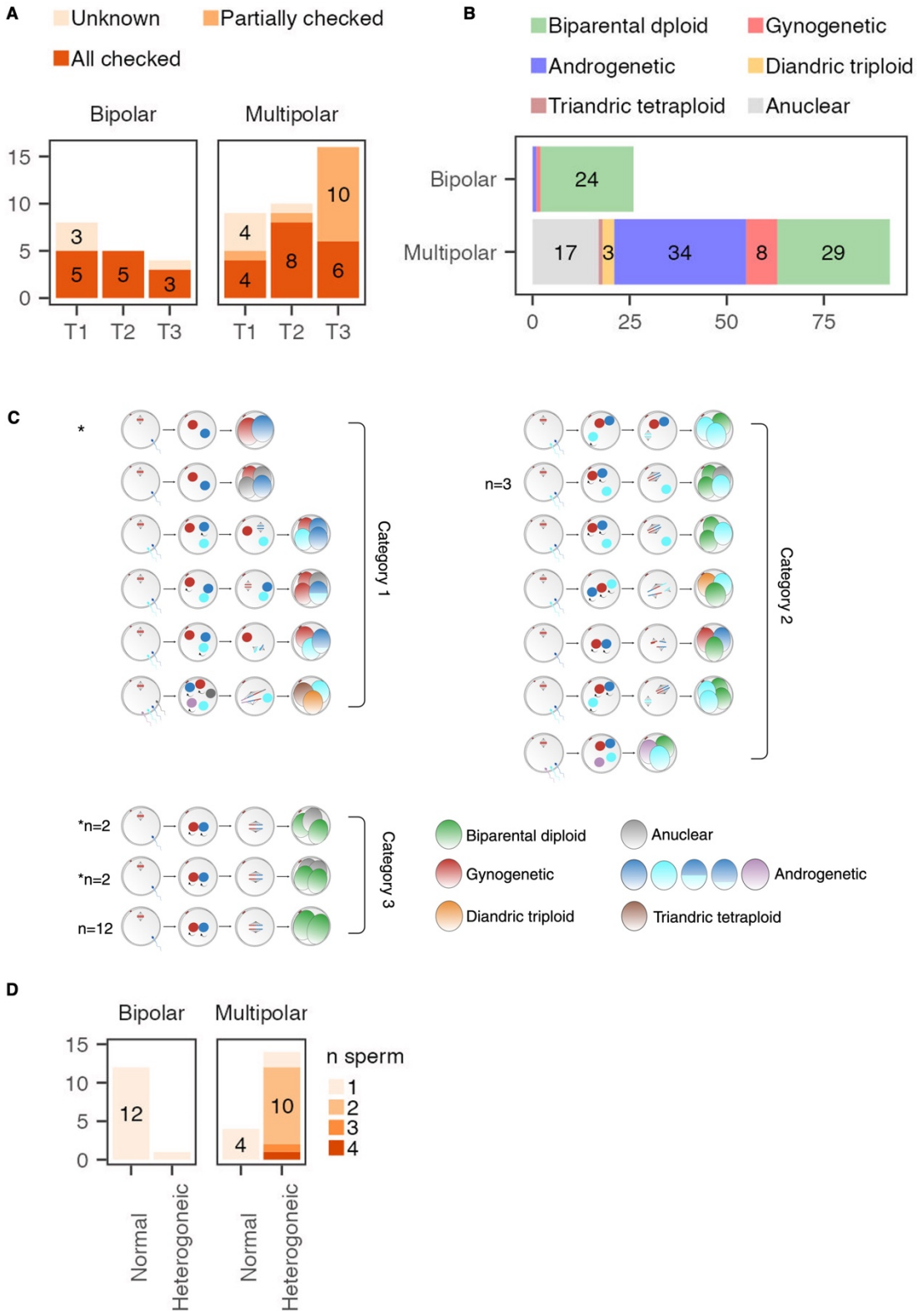

Figure 2. Whole-genome segregation errors occur in multipolar and bipolar first cleavages. (A) Numbers of bipolar and multipolar cleaving embryos used for each blastomere culturing timepoint, categorized based on the completeness of embryo-derived blastomere outgrowth haplotyping: fully haplotyped (All checked), partially haplotyped (Partial), or not haplotyped (Unknown). (B) The inferred chromosomal constitution of 118 blastomeres in culture. (C) Three

categories of genome segregation patterns identified during the first cleavage. In the oocyte being fertilized, the second meiotic division is depicted, along with the likely number of sperms fertilizing the embryo as deduced from the haplotypes. The arrows surrounding the pronuclei indicate replication occurred. During the first cleavage, spindles segregating the sister chromatids are shown. In the absence of a spindle, the genome is extruded. Numbers are given for patterns that occurred more than once. * in category 1 indicates the one embryo with bipolar first cleavage and WG segregation error. * in category 3 indicates the four embryos with multipolar first cleavage and without WG segregation error. For androgenetic blastomeres, different colors indicate genetic material from different sperm. (D) Chromosomal segregation patterns for embryos with bipolar or multipolar first cleavage and the inferred number of sperm that fertilized the egg. Normal: Zygote cleaved without WG segregation error. Heterogoneic: Zygote cleaved with WG segregation error. Bipolar and multipolar refer to embryos undergoing either bipolar or multipolar first cleavage, respectively.

For the 31 fully checked embryos, genome composition of all cultured blastomeres allowed us to reconstruct genome segregation patterns during the first cleavage. We observed three broad categories of genome segregation patterns during the first cleavage (**Fig. 2C; Supplemental Table S1**). Category 1 contains 6 embryos with all blastomeres harboring WG abnormalities. Category 2 comprises 9 embryos with a mixture of blastomeres, some with WG abnormalities and others being biparental diploid. Category 3 consists of 16 embryos with only biparental diploid blastomeres. The four multipolar cleaving zygotes in this category also produced anuclear cells. Among the 31 fully examined embryos, 78% (14 out of 18) of those with multipolar first cleavage demonstrated heterogoneic division, while only 8% (1 out of 13) of embryos with bipolar first cleavage showed WG segregation errors (p=0.00048) (**Fig. 2C**), confirming the enrichment of heterogoneic division in multipolar cleaving zygotes(De Coster et al. 2022). Furthermore, the high frequency of polyspermic conceptions in embryos undergoing multipolar first zygotic division and exhibiting WG segregation errors(De Coster et al. 2022) was validated, with 86% (12 out of 14) of these embryos

174 inferred to be fertilized by more than one sperm. In contrast, all other embryos with
175 bipolar first cleavage or with multipolar first cleavage but without WG segregation
176 errors were inferred to be fertilized by a single sperm (**Fig. 2D**). Only 10% (1 out of 10)
177 of dispermic embryos give rise to triploid blastomeres, which is consistent with previous
178 observations that dispermic fertilization seldom leads to triploid development(De
179 Coster et al. 2022; Kola et al. 1987). Most of the observed mechanisms driving
180 heterogoneic division align with those from our previous study(De Coster et al. 2022;
181 Destouni et al. 2016). Among the 15 embryos undergoing heterogoneic division, 10
182 were inferred to involve the extrusion of paternal pronuclei into separate cells, 4 likely
183 involved an independent spindle separating paternal or maternal chromosomes, 2
184 likely involved a tripolar spindle, and 1 likely involved double spindles (**Fig. 2C**).

185 Interestingly, two novel genome segregation mechanisms were identified. Firstly, within
186 category 1, we observed an embryo undergoing bipolar first cleavage, yet exhibiting
187 heterogoneic division (**Fig. 2C**). The most plausible explanation is that the two parental
188 zygotic spindles failed to align and instead segregated into distinct blastomeres. Hence,
189 genome-wide segregation errors are not confined to multipolar cleavers. Additionally,
190 within category 3, we identified four embryos undergoing multipolar first cleavage, yet
191 exhibiting normal genome segregation. Specifically, two biparental diploid blastomeres
192 were generated alongside one or two anuclear cells (**Fig. 2C**). These findings suggest
193 that bipolar first cleavage does not always ensure normal genome segregation, and
194 multipolar first cleavage does not inevitably result in WG or chromosomal segregation
195 errors.

196 **Blastomeres with whole-genome abnormalities can reach blastocyst stage**
197 **despite impaired developmental potential**

198 To investigate the developmental potential of heterogoneic division-derived
199 blastomeres with WG abnormalities, we compared the developmental stage of the 53
200 biparental diploid blastomere outgrowths and 48 blastomere outgrowths with WG
201 abnormalities at the time of outgrowth collection (**Fig. 3A,B)**. We observed impaired
202 development for blastomeres with WG abnormalities compared to biparental diploid
203 blastomeres at T3, with 80% (12 out of 15) of biparental diploid blastomere outgrowths
204 developing to blastocysts, while only 21% (6 out of 28) of blastomere outgrowths with
205 WG abnormalities reached this stage (p=0.0016) (**Fig. 3B,C**).

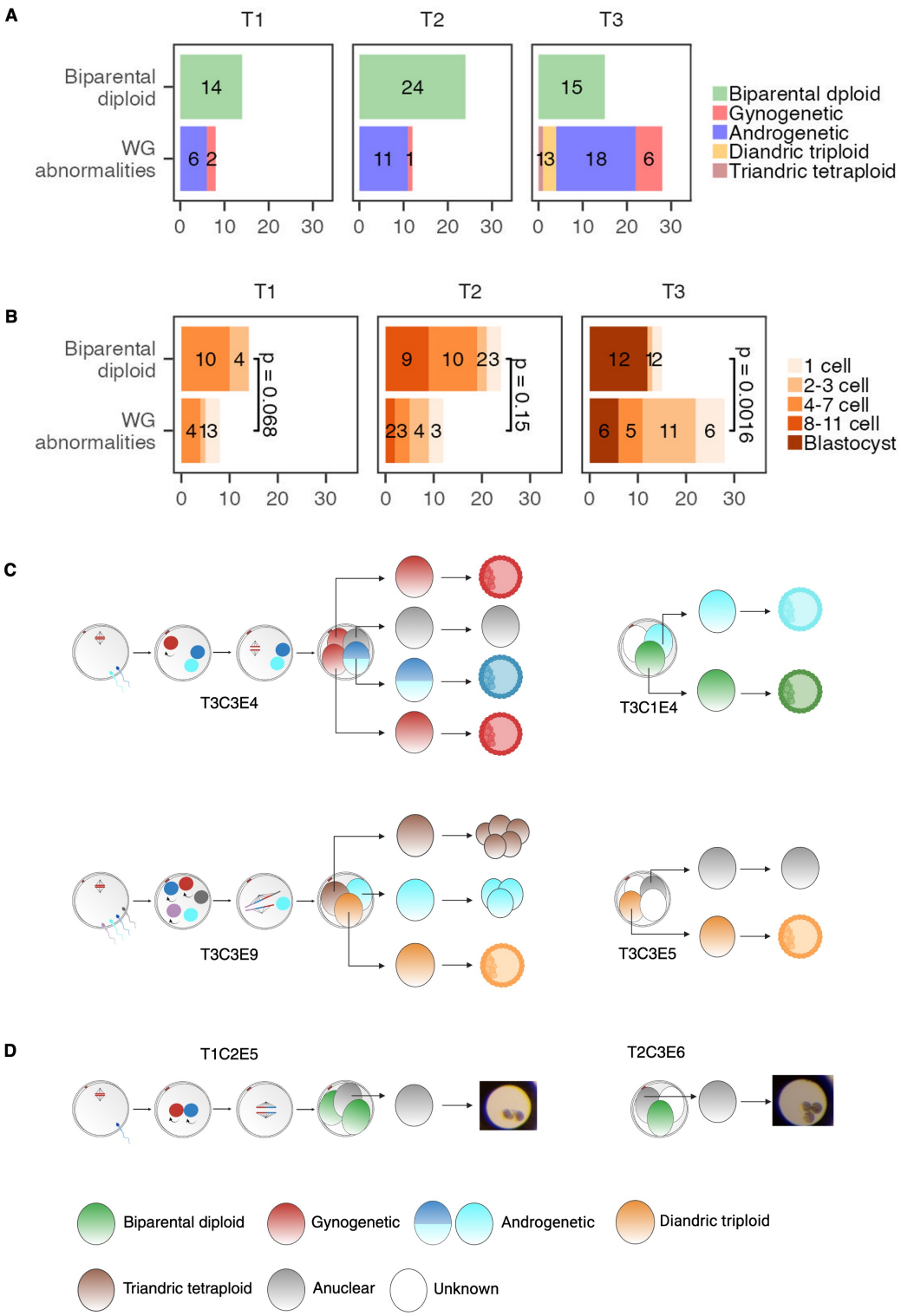

Figure 3. Blastomeres with whole-genome abnormalities can reach blastocyst stage despite impaired developmental potential. (A) Distribution of 53 biparental diploid blastomere outgrowths and 48 blastomere outgrowths with WG abnormalities across different timepoints of outgrowth collection. (B) Developmental stage comparison of biparental diploid blastomere outgrowths and blastomeres outgrowths with WG abnormalities in (A). (C) Schematic representation of the six blastomere outgrowths with WG abnormalities that reached the blastocyst stage at T3, along with their sibling blastomere outgrowths and original embryos. (D)

Images of the two cleaved anuclear blastomere outgrowths and schematic diagrams illustrating the embryos from which they originated. In (C) and (D), the same symbols as in Figure 2C are employed. Fertilization and the first cleavage are not depicted for embryos containing blastomeres with an unknown haplotype (due to sample loss or haplotype failure).

Since aneuploidy is known to affect embryo development, we next evaluated the impact of heterogoneic division on aneuploidy levels in daughter blastomeres. By comparing the aneuploidy spectrum of blastomeres from both normal genome segregation and heterogoneic division, we observed a lower proportion of euploid blastomeres and a higher proportion of blastomeres with high-level aneuploidy (defined as >10% of autosome regions being aneuploid, with 10% corresponding to two large chromosomes) in blastomeres from heterogoneic division, compared to blastomeres originating from zygotes with normal genome segregation (**Supplemental Fig. S1**). Specifically, for blastomeres with WG abnormalities resulting from heterogoneic division, 32% (10 out of 31) were euploid, while 55% (17 out of 31) displayed high level aneuploidy. In contrast, for blastomeres from normal genome segregation, 56% (18 out of 32) were euploid, and only 3% (1 out of 32) exhibited high level aneuploidy (p=6.3×10^{-6}) (**Supplemental Fig. S1**). Similarly, other studies demonstrated the increased rate of complex chromosomal abnormalities for embryos with multipolar division(Zhan et al. 2016; Daughtry et al. 2019). The association between heterogoneic division and vulnerability to chaotic chromosomal missegregations might be caused by the spindle abnormalities implicated in this process (Chatzimeletiou et al. 2005) **(Fig. 2C**). To control for the effect of aneuploidy on blastomere development, we compared the development of only euploid blastomeres. At T3, all biparental diploid blastomere outgrowths (100%,12 out of 12)

238 reached blastocyst stage, while a much lower proportion (36%, 4 out of 11) of
239 blastomere outgrowths with WG abnormalities reached blastocyst stage (p=0.0013).
240 Additionally, for androgenetic blastomere outgrowths collected at T3, 2 out of 15
241 containing the X chromosome reached the blastocyst stage, while the 3 without the X
242 chromosome did not, indicating that the Y chromosome alone is insufficient for
243 blastocyst formation.

244 The majority of the 17 anuclear blastomeres arrested at the 1-cell stage. However, we
245 identified 2 exceptions: one reached the 2-cell stage at T1, and the other reached the
246 3-cell stage at T2 (**Fig. 3D**), suggesting that the cytoplasmic divisions could occur
247 without a nucleus. Additionally, we identified 16 more anuclear biopsies from 14 non-
248 anuclear blastomere outgrowths at various stages of development, with the majority of
249 the original blastomeres (12 out of 14) from embryos underwent multipolar first
250 cleavage (**Supplemental Table S2**). Hence, the formation of anuclear blastomeres is
251 not restricted to the first zygotic division. To confirm the origin of these empty
252 outgrowths/biopsies, we examined the mitochondrial genotypes for empty biopsies
253 obtained from the same cows. Maternal inheritance of the mitochondrial genome was
254 corroborated by similar mitochondrial genotypes (**Supplemental Table S3**).

255 To conclude, blastomeres with WG abnormalities from heterogoneic division show
256 diminished development. Despite this, certain uniparental/polyploid blastomeres still
257 progress to the blastocyst stage (**Fig. 3C**), indicating their viability during the
258 preimplantation stage and raising concerns about their further development and
259 potential contribution to abnormal pregnancies.

260 **Whole-genome abnormalities do not alter the preimplantation developmental**
261 **program but hinder transcriptomic development**

262 We hypothesized that the impaired development of blastomere outgrowths with WG
263 abnormalities would be reflected in the transcriptomic profiles of constituent cells, with
264 WG abnormalities potentially causing deviations in the preimplantation developmental
265 program. To investigate the effects of WG abnormalities on transcriptomic
266 development, we conducted single-cell transcriptome sequencing on 677 cells derived
267 from collected blastomere outgrowths. Among these, 446 transcriptomes met our
268 quality control criteria, representing cells from 124 blastomere outgrowths derived from
269 49 embryos (**Supplemental Table S2; Methods**). We noted significantly higher
270 fractions of mitochondrial transcripts in cells from blastocyst stage outgrowths
271 compared to cells from other stages, except the 1-cell stage (**Supplemental Fig. S2**).
272 The blastocyst stage cells with high fraction of mitochondrial transcripts were not
273 enriched for cells with WG abnormalities. This finding suggests active mitochondrial
274 gene expression in blastocysts and potential cytoplasmic RNA leakage in arrested 1-
275 cell stage outgrowths. Consistent with our findings, previous studies utilizing PCR
276 analysis have demonstrated a significant increase in mitochondrial transcripts at
277 morula and blastocyst stages across various mammalian species(Ma et al. 2008; May-
278 Panloup et al. 2005; Thundathil et al. 2005).

279 Following dimensionality reduction with Unified Manifold Approximation and Projection
280 (UMAP), single-cell gene expression profiles exhibited a developmental trajectory from
281 T1 to T3 (**Fig. 4A**). Cells with WG abnormalities did not form distinct clusters (**Fig. 4B**).

282 Instead, by checking the expression of marker genes for essential preimplantation
283 stages, we identified clusters corresponding to minor EGA, major EGA, inner cell mass
284 (ICM), and trophectoderm (TE) stages, which we define as the molecular
285 developmental stages of the cells. The cell cluster without EGA (pre-EGA) contained
286 cells arrested before EGA (**Fig. 4C; Supplemental Fig. S3**). Pseudotime analysis with
287 single-cell transcriptome data inferred developmental trajectories pointing to ICM and
288 TE (**Fig. 4D**). These results indicate that transcriptomic changes are mainly driven by
289 the natural developmental program rather than variations in genome constitution,
290 aligning with previous single-cell transcriptome analyses of uniparental(Leng et al.
291 2019) and aneuploid(Fernandez Gallardo et al. 2023) cells from human
292 preimplantation embryos.

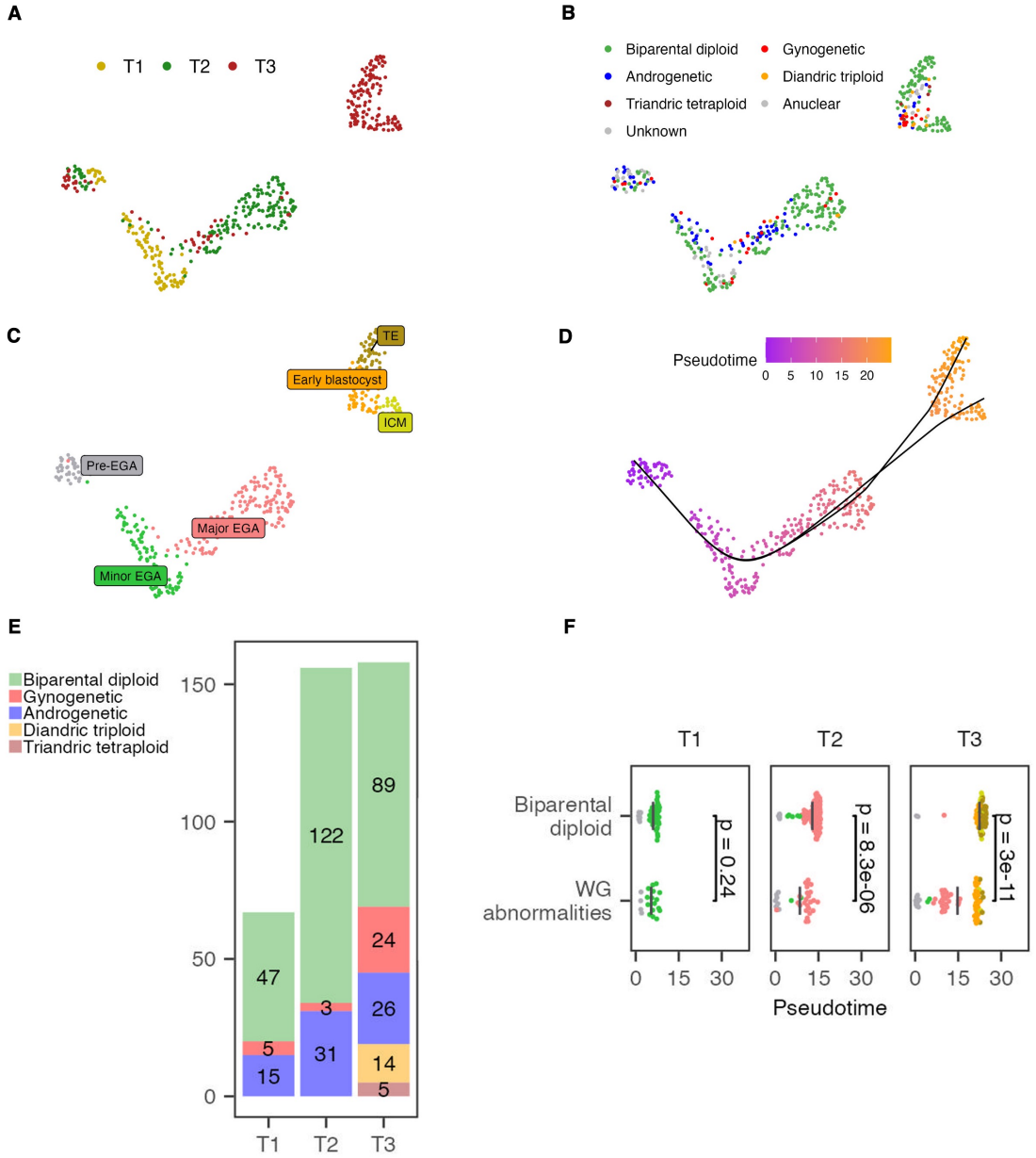

Figure 4. Whole-genome abnormalities do not alter the preimplantation developmental program but hinder transcriptomic development. UMAP for single-cell transcriptome data with cells colored by (A) time of outgrowth collection (B) genome constitution (C) molecular developmental stage indicated by marker genes expression (D) pseudotime value inferred from trajectory analysis. The inferred pseudotime trajectories are indicated by black curved lines on the UMAP. (E) Number of biparental diploid cells and cells with WG abnormalities used for transcriptome analysis for each timepoint. (F) Pseudotime comparison of biparental diploid cells and cells with WG abnormalities at each outgrowth collection timepoint. Each dot represents one cell, with the x-axis indicating its pseudotime value extracted from (D). Cells are colored according to their corresponding molecular developmental stage in (C) using the same color scheme. Vertical grey bars indicate the mean pseudotime value of each group.

We then explored whether the impaired development of blastomeres exhibiting WG

306 abnormalities was reflected in single-cell transcriptome profiles. We characterized the
307 physical age of the cells based on the time of outgrowth collection, while their
308 molecular age was assessed using pseudotime values along the transcriptional
309 trajectory. Compared to cells from biparental diploid outgrowths, those from outgrowths
310 displaying WG abnormalities exhibited impaired development at T2 and T3, as
311 evidenced by their smaller transcriptome-pseudotime ages (**Fig. 4E,F**; $p=4.5\times10^{-5}$ for
312 T2 and $p=4\times10^{-10}$ for T3). This trend persisted when considering only cells inferred to
313 be euploid ($p=0.00026$ for T2 and $p=0.039$ for T3). Our observation indicates the cell-
314 level impaired transcriptomic development of blastomeres with WG abnormalities
315 starting form T2, coinciding with major EGA.

316 Some blastomere outgrowths collected at T2 or T3 did not have the expected number
317 of cells and appeared to be cleaving slower or blocked in their development.
318 Surprisingly, when mapping the transcriptome profiles on the developmental
319 trajectories, we observed that some cells from 1 cell and 2-3 cell stage outgrowths at
320 T3 displayed profiles resembling major EGA, while some cells from 4-7 cell outgrowths
321 exhibited profiles akin to TE or ICM (**Supplemental Fig. S4**). These observations
322 suggest that transcriptomic development can continue in the absence of cell divisions.

323 **Distinct preimplantation cellular states are governed by specific key**
324 **transcription factors**

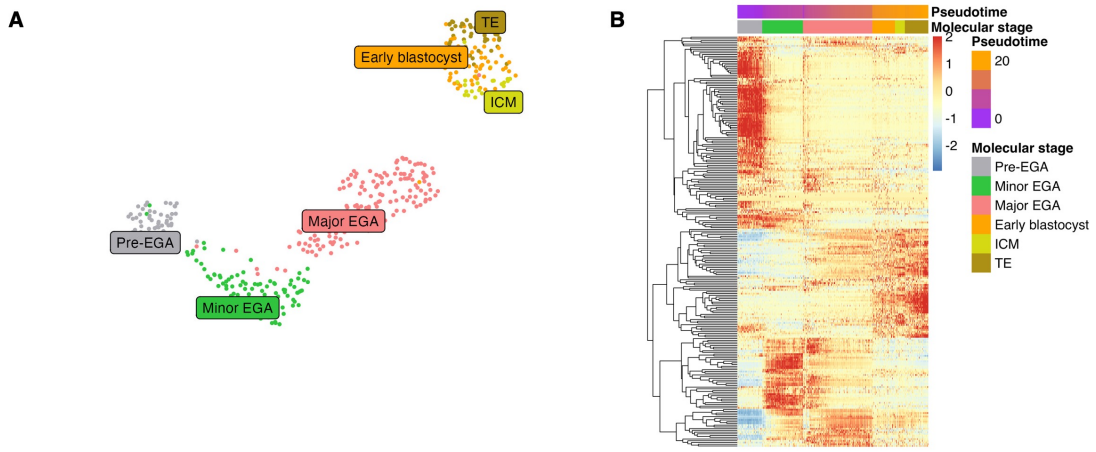

C

Molecular stage	Selected key regulons
Pre-EGA	SIX3, PRDM5, ZBTB43, SMC3, EBF1, HES7
Minor EGA	KLF17, MAX, ZNF143, THAP11, CHD1, IRF3
Major EGA	MITF, ARNT, RARB, HSF1, USF1, BRCA1
Early blastocyst	GATA2, TBX3
ICM	SOX15, NELFB, SREBF1, GATA6, ERF, MAZ
TE	CDX2, TCF7L1, JDP2, JUN, GATA2, GATA3

Figure 5. Distinct preimplantation cellular states are governed by specific key transcription factors. (A) UMAP displaying cell clustering based on regulon activity, with cells colored according to their macular developmental stage as depicted in Figure 4C. (B) Heat map of regulon activity. Each row represents one regulon and each column represent one cell. The plot is generated using rescaled Area Under the Curve (AUC) values, with cells ordered according to their molecular developmental stage and pseudotime values. (C) Key regulons selected for each stage.

Since cells were clustered according to their molecular developmental stage regardless of genome composition, we next aimed to uncover the specific gene regulatory networks (GRNs) shaping cellular identity at each stage. We used pySCENIC to infer GRNs from single-cell RNA-seq data, based on co-expression of TFs and their target genes as well as cis-regulatory motif analysis. This approach identified 237 regulons, each comprising a transcription factor (TF) alongside its predicted target genes. Subsequently, we generated a UMAP visualization based on regulon activity, partitioning cells into distinct regulatory states (**Fig. 5A**). As anticipated,

341 cells belonging to same molecular stage exhibited clustering, indicative of stage-
342 specific regulatory dynamics. To further investigate the coactivity of TF combinations
343 within each stage, we ordered cells based on their molecular stage and pseudotime
344 values on regulon activity heatmap. The resulting plot revealed stage-specific
345 regulatory states characterized by the activation or repression of specific TFs (**Fig. 5B**).
346 We then selected key regulons with both high activity and specificity for each stage
347 (**Fig. 5C; Supplemental Fig. S5; Methods**). Most of the TFs for selected key regulons
348 have been shown to be crucial for embryonic development (**Supplemental Table S4**).
349 For instance, GATA6 has demonstrated significance in the ICM of mouse, bovine, and
350 human embryos(Niakan and Eggan 2013; Marsico et al. 2023). Similarly, CDX2,
351 GATA2 and GATA3 have been implicated in the TE of mouse, bovine and human
352 embryos(Home et al. 2017; Fernandez Gallardo et al. 2023; Gerri et al. 2020;
353 Nagatomo et al. 2013; Niakan and Eggan 2013; Negrón-Pérez et al. 2017).
354 Interestingly, for the pre-EGA stage, PRDM5 was identified as a key regulon, reflecting
355 the arrested characteristics of these cells, as this TF is involved in G2/M arrest and
356 apoptosis through suppressing the expression of several oncogenes and antagonizing
357 WNT/β-catenin signaling(Deng and Huang 2004; Shu et al. 2011). These findings shed
358 light on the combinations of TFs that underlie cell state transitions and cellular identity
359 during bovine preimplantation embryogenesis.

360 **Whole-genome abnormalities induce stress responses during embryonic**
361 **genome activation**

362 Although WG abnormalities did not result in obvious deviations in the preimplantation

363 developmental program, we hypothesized that the imbalanced parental genome
364 compositions in cells with WG abnormalities could lead to parent-specific gene
365 expression patterns for genes predominantly expressed from only one parent's
366 genome. Furthermore, these WG abnormalities may function as stress stimuli,
367 inducing global transcriptomic changes that ultimately impair the overall developmental
368 potential of cells. To investigate the parental genome-specific effects on gene
369 expression, we compared the gene expression profiles of gynogenetic, androgenetic,
370 and polyploid (diandric triploid and triandric tetraploid) cells to those of biparental
371 diploid cells within each molecular developmental stage. Additionally, to capture the
372 overall effects of WG abnormalities on gene expression, we aggregated all cells with
373 WG abnormalities for combined analyses.

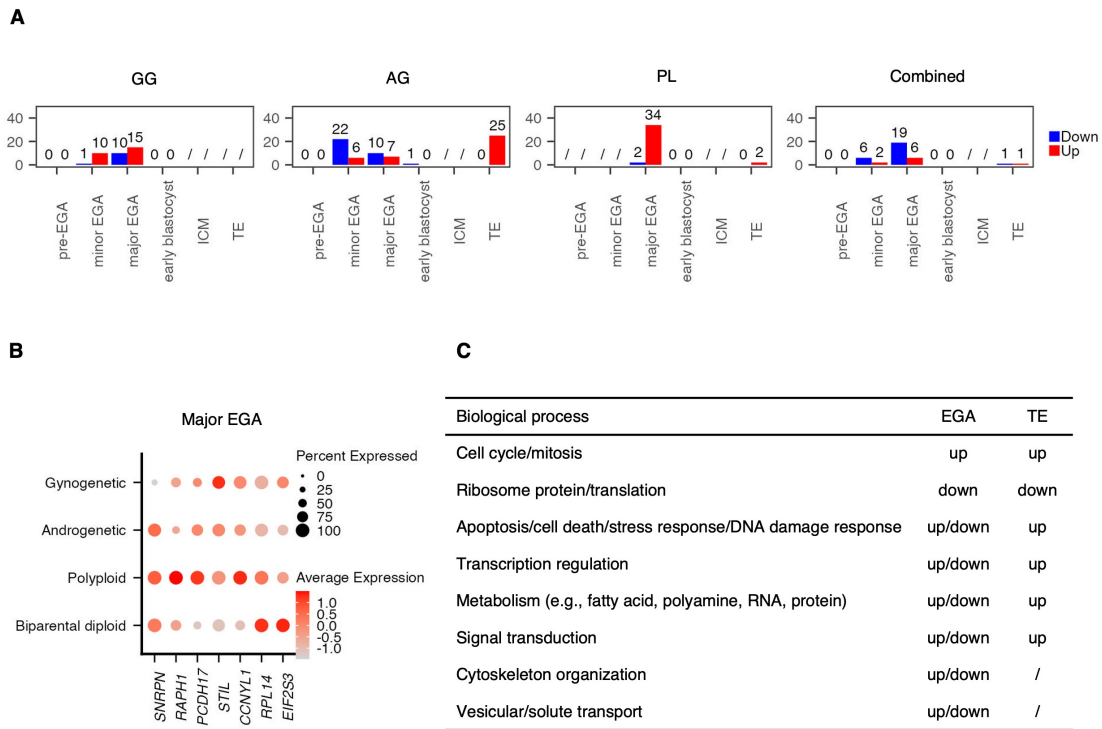

Biological process	EGA	TE
Cell cycle/mitosis	up	up
Ribosome protein/translation	down	down
Apoptosis/cell death/stress response/DNA damage response	up/down	up
Transcription regulation	up/down	up
Metabolism (e.g., fatty acid, polyamine, RNA, protein)	up/down	up
Signal transduction	up/down	up
Cytoskeleton organization	up/down	/
Vesicular/solute transport	up/down	/

374

375 **Figure 6.** Whole-genome abnormalities induce stress responses during embryonic genome
376 activation. (A) Numbers of DE genes identified in gynogenetic (GG), androgenetic (AG),
377 polyploid (PL) and combined WG-aberrant cells compared to biparental diploid cells for each

stage. The "/" symbol denotes comparisons not conducted due to insufficient cells. (B) Gene expression dot plot for example DE genes during major EGA. (C) Overall alterations in biological processes reflected by deviations in gene expression. "/" if no DE genes observed.

Differentially expressed (DE) genes were identified from the onset of EGA (**Fig. 6A**), suggesting that WG abnormalities lead to gene expression changes during EGA. Only one DE gene was identified at the early blastocyst stage, indicating a high degree of similarity between normal cells and cells with WG abnormalities just before the first lineage specification. DE genes found in the combined analysis partially overlap with those identified in separate analyses **(Supplemental Fig. S6; Supplemental Table S5)**. Manual functional annotation revealed some parental genome specific effects. We noted the downregulation of the maternally imprinted gene *SNRPN* in gynogenetic cells during major EGA, aligning with its known paternal-specific expression(Lucifero et al. 2006). Furthermore, we identified the up regulation of genes involved in cell adhesion (e.g., *RAPH1, PCDH17*) in polyploid cells during major EGA and at the TE stage (**Fig. 6B; Supplemental Table S5**). This indicates active cell adhesion-related processes, such as compaction in these cells, possibly caused by the additional paternal genome contribution.

Other DE genes observed in uniparental/polyploid cells, as well as those identified through combined analysis, are mainly involved in similar biological processes, indicating global effects of WG abnormalities (**Fig. 6C; Supplemental Table S5**). We observed upregulation of cell cycle/mitosis-related genes (e.g., *STIL*, *CCNYL1*), indicating active preparation for cell cycle progression in cells with WG abnormalities. Meanwhile, we noted downregulation of ribosomal protein genes (e.g., *RPL14*) and

401 translation initiation factor genes (e.g., *EIF2S3*). It is known that during cellular
402 adaptation to stress stimuli, growth-related genes, including those involved in
403 ribosomes and translation, are typically repressed, prioritizing resources towards
404 stress protection over rapid proliferation(López-Maury et al. 2008). Our observation
405 indicates reduced growth in cells with WG abnormalities as a consequence of the
406 stress response triggered by WG abnormalities. Interestingly, for certain biological
407 processes, DE genes were identified during EGA, leading to either upregulation or
408 downregulation of these processes. No relevant DE genes were found for the early
409 blastocyst stage, while in the TE, no DE genes or only DE genes resulting in
410 upregulated activities of these processes were observed. The biological processes
411 involved include apoptosis, cell death, stress response, DNA damage response,
412 transcription regulation, metabolism, single transduction, cytoskeleton organization
413 and transport **(Fig. 6C; Supplemental Table S5).** This indicates that cells with WG
414 abnormalities adapt to stimuli caused by genome imbalance through transcriptional
415 responses during EGA, involving transient upregulation or downregulation of relevant
416 genes(López-Maury et al. 2008). A quiescent period follows during the early blastocyst
417 stage, while the upregulation of specific genes in TE reflects establishment of new
418 steady-state levels. Additionally, we conducted differential regulon analysis and DE
419 regulons were identified for cells with WG abnormalities only during EGA
420 (**Supplemental Table S5**). Most DE regulons are essential for embryonic development
421 and their bidirectional changes mirror bidirectional gene expression alterations
422 observed in differential gene expression analysis (**Supplemental Table S5**).

423 In summary, we observed parental genome-specific effects induced by WG
424 abnormalities, suggesting distinct roles of the maternal and paternal genomes.
425 Moreover, we identified universal cellular responses to WG abnormalities, marked by
426 active preparation for cell cycle progression alongside reduced cell growth.
427 Bidirectional alterations in specific biological processes and regulons during EGA, and
428 their eventual balance, may dictate whether cells arrest or advance towards the
429 blastocyst stage. Overall, these observed stress responses provide insights into the
430 impaired development cause by WG abnormalities.

431 **Discussion**

432 WG abnormalities are a type of chromosomal error frequently observed in
433 spontaneous abortions(Hassold et al. 1980) and on very rare occasions in a chimeric
434 state in live-born individuals(Madan 2020). Contrary to its implications in abnormal
435 pregnancy and congenital abnormalities, the proposed origins of such anomalies are
436 deductions from surviving cells at later stages or remain speculative, and their effect
437 on early development remains largely unknown. Here, we provide fundamental
438 insights into the natural emergence and early developmental biology of gynogenetic,
439 androgenetic, and polyploid blastomeres using haplotyping and single-cell
440 transcriptome analysis. We demonstrated the spontaneous occurrence of uniparental
441 and polyploid blastomeres through a non-canonical division during the first zygotic
442 cleavage, which segregates parental genomes into distinct blastomeres. We not only
443 confirmed our previous observation(De Coster et al. 2022) that heterogoneic division
444 mostly coincides with multipolar first cleavage in polyspermic embryos, but also

445 identified, for the first time, heterogoneic division occurring with bipolar first cleavage
446 in normally fertilized embryos. The reduced developmental potential of uniparental and
447 polyploid blastomeres derived from heterogonic division was evidenced by a lower
448 blastocyst rate and a delay in pseudotime values beginning from T2, coinciding with
449 major EGA. Stress responses observed during EGA suggests the cells' efforts to
450 combat fitness challenges induced by aberrant genome composition, with the outcome
451 determining whether they arrest or progress to the blastocyst stage.

452 Although to our knowledge we are the first to explore the development of first-
453 cleavage-derived uniparental and polyploid blastomeres, some studies have examined
454 the preimplantation development of mammalian uniparental embryos. These embryos
455 were generated through various methods, including nuclear manipulation(Leng et al.
456 2019; Hoppe and Illmensee 1977; Xu et al. 2021), *in vitro* induction (Leng et al. 2019;
457 Hao et al. 2004; Hwang et al. 2020; Ito et al. 1991; Liu et al. 2002) or natural
458 occurance(Hardy et al. 1989) of parthenogenetic development in unfertilized oocytes,
459 as well as bisection of one-cell fertilized eggs (Tarkowski 1977). Aligned with the
460 impaired developmental potential observed in blastomeres with WG abnormalities in
461 our study, those studies on preimplantation uniparental embryos have shown a
462 decrease in the morula/blastocyst rate compared to biparental diploid embryos.,
463 alongside poorer morphology and reduced cell count in resulting blastocysts(Hardy et
464 al. 1989; Leng et al. 2019). Several studies have monitored post-implantation
465 development and affirmed the compatibility of diploid uniparental genome constitution
466 with later development. For instance, porcine parthenogenetic fetuses can develop

467 until day 35 with abnormal organ morphologies (Hwang et al. 2020). Additionally, live-
468 born fertile mice have been created via both androgenesis and gynogenesis(Hoppe
469 and Illmensee 1977). Moreover, diploid gynogenetic cells have been identified in
470 various organs of live-born chimeric mice developed from aggregated chimeric
471 embryos(Ito et al. 1991). These findings are consistent with observations in humans,
472 suggesting that uniparental cell lines are typically selected against during development
473 but can persist until late pregnancy and even be compatible with live birth, raising
474 various concerns. Our study demonstrates that heterogoneic division could serve as a
475 spontaneous origin of uniparental and polyploid cell lines observed during late
476 development.

477 The parental genome specific effects identified in this study correlates with findings
478 from a prior investigation of uniparental human embryos(Leng et al. 2019). As for the
479 stress response observed solely in our study, there are possible causes aside from
480 species-specific effects and sample variations(Xu et al. 2021). The referenced study
481 created diploid gynogenetic and androgenetic embryos through nuclear manipulation
482 and induction of parthenogenesis, respectively. Only embryos demonstrating good
483 morphology and developmental speed were utilized. Only XX and XY androgenetic
484 embryos were included. And their analysis focused exclusively on genes with highly
485 biased expression in gynogenetic or androgenetic embryos. In contrast, our study
486 focused on a broad spectrum of spontaneously occurring WG abnormalities, which
487 frequently exhibit complex aneuploidy and contain either haploid or diploid genome
488 constitutions. While haploidy has been demonstrated to convert frequently to diploidy

489 during development(Tarkowski 1977; Ito et al. 1991; Leng et al. 2017), both complex
490 aneuploidy and haploidy are known to impact preimplantation development(Liu et al.
491 2002; McCoy et al. 2015). Additionally, our cohort included androgenetic blastomeres
492 lacking the X chromosome, a condition known to cause embryonic arrest. Finally,
493 rather than focusing solely on genes with highly biased expression in gynogenetic or
494 androgenetic embryos, our study examined the broader impact of WG abnormalities
495 on global gene expression changes. These factors led us to observe EGA as a critical
496 period for embryos with WG abnormalities. During this stage, their constituent cells
497 exhibit stress responses in gene expression, which could determine whether they
498 arrest or successfully progress to the blastocyst stage.

499 We identified anuclear cells from outgrowth at different stages, which is in agreement
500 with previous observations in rhesus(Daughtry et al. 2019) and human embryos(Hardy
501 et al. 1993). Consistent with our previous analysis(De Coster et al. 2022), most of the
502 anuclear blastomeres were identified from blastomere outgrowths following multipolar
503 first cleavage, suggesting a potential association between the first cleavage pattern
504 and the origin of these anuclear cells. In addition, we demonstrate that some of the
505 anuclear cells can cleave without nuclei. Cytoplasmic divisions are generally thought
506 to rely on nuclear divisions and mitotic signals. However, a recent study by Bakshi et
507 al. observed that cytoplasm can compartmentalize, and a rare fraction of the
508 compartments can divide repeatedly without nuclei and independent of mitotic
509 CDK/cyclin complexes during normal drosophila embryogenesis (Bakshi et al. 2023).
510 They showed that this phenomenon is relevant to mitotically delayed nuclei. We

511 hypothesize that a similar mechanism may apply here, with the anuclear cells derived
512 from mother cells containing nuclei with delayed mitosis. These findings collectively
513 underscore the need for further investigation into the detailed mechanisms underlying
514 the presence of anuclear cells in mammalian embryos and their potential roles in
515 embryo development.

516 Insights from this study raise clinical concerns. Firstly, in IVF laboratories, human
517 embryos with two pronuclei (PN) are preferentially selected for transfer(Balaban et al.
518 2011). We demonstrate here that zygotes with three PN may result in a mixture of
519 biparental diploid and uniparental/polyploid blastomeres. Since the latter are
520 developmentally compromised, the resulting embryo may still develop normally.
521 Secondly, there is a growing trend in many laboratories to monitor embryonic
522 development using time-lapse microscopy and rank embryos based on cleavage
523 kinetics(Sugimura et al. 2017, 2012; Sigalos et al. 2016; Balaban et al. 2011). Embryos
524 with multipolar first cleavage are typically given a low rank. We showed here that 22%
525 of embryos with a multipolar first cleavage exhibited normal, equal division of the
526 genome with additional anuclear cells. It would be unjust to low rank these embryos
527 since they have the potential to lead to healthy babies. Additionally, even though
528 uniparental/polyploid cells are normally generated with multipolar first cleavage, it is
529 not uncommon that biparental diploid blastomeres are generated together, which may
530 gain developmental advantage and lead to normal development. Thirdly, embryos
531 typically ranked high, characterized by a normal pronuclei count and bipolar first
532 cleavage, may still experience WG segregation errors, leading to the generation of

533 solely uniparental cells, posing a potential risk of abnormal pregnancy. Rather than
534 removing or keeping embryos based on apparent abnormalities, it might be better to
535 evaluate the genome constitution of preimplantation embryos and deselect those with
536 WG abnormalities, while retaining those with a normal chromosome count and parental
537 haplotype constitution. Preimplantation genetic testing for aneuploidy (PGT-A) has
538 become a common practice to select embryos with a normal number of chromosomes
539 for transfer. However, the majority of PGT-A tests only measure aneuploidies, with
540 only some measuring the parental haplotype constitution(Coonen et al. 2020). We
541 suggest the use of genotyping/haplotyping together with PGT-A(Masset et al. 2022;
542 Zamani Esteki et al. 2015) to check both chromosome count and parental haplotype
543 constitution and select against WG abnormalities. This approach is likely to further
544 improve the overall IVF success rate(Caroselli et al. 2023).

545 In conclusion, this study provides comprehensive insights into the natural origin and
546 early development of uniparental/polyploid blastomeres. We demonstrated their
547 overall impaired developmental potential, primarily due to stress responses triggered
548 by WG abnormalities during EGA. Blastomeres that successfully navigate through this
549 phase and progress to the blastocyst stage may constitute a significant fraction of
550 embryos and contribute to abnormal development. Our findings underscore the
551 importance of routine screening against embryos bearing WG abnormalities in IVF labs.

552 **Methods**

553 **Single-cell collection from bovine blastomere outgrowths**

554 *In vitro embryo production*

555 Prior ethical agreement was not necessary. Ovaries from cows raging 4 to 5 years
556 were collected post-mortem in a commercial slaughterhouse. The sperm used for *in*
557 *vitro* fertilization was collected from a 5-years-bull. Standard in vitro procedures were
558 followed to produce bovine embryos (Wydooghe et al. 2014). Briefly, bovine (*Bos*
559 *taurus*) ovaries were collected and processed within 2 h. The ovaries were rinsed three
560 times in warm physiological saline supplemented with 0.25µg/mL kanamycin. Using an
561 18-G needle and a 10-mL syringe, antral follicles (2 – 8 mm diameter) were punctured
562 and kept separately per ovary in 2.5 mL Hepes-Tyrode's albumin-pyruvate-lactate
563 (Hepes-TALP). Using a stereomicroscope, cumulus-oocyte complexes were collected
564 and washed in Hepes-TALP and then in maturation medium (modified bicarbonate-
565 buffered TCM-199 supplemented with 50 ppm gentamicin and 20 ng/mL epidermal
566 growth factor). Cumulus-oocyte complexes were *in vitro* matured per donor in four-well
567 dishes (NuncTM) in 500 µL maturation medium for 22 h at 38.5°C in 5% CO_2 in
568 humidified air. *In vitro* fertilization was performed with frozen-thawed semen from a
569 Holstein-Friesian bull (*Bos taurus*) after selection over a discontinuous 45/90%
570 Percoll® gradient (GE Healthcare Biosciences, Uppsala, Sweden). The mature oocytes
571 were fertilized by incubating them with spermatozoa at a concentration of 1×10^6
572 spermatozoa/mL in IVF–TALP medium enriched with BSA (Sigma A8806; 6 mg/mL)
573 and heparin (20 µg/mL) for 21 hours at 38.5°C, 5% CO_2 in humidified air. After
574 fertilization, the presumed zygotes were vortexed in 2.5 mL HEPES-TALP for 3 minutes
575 to remove the cumulus and sperm cells adhered to the *zona pellucida* and

576 subsequently transferred to 50 µL droplets of synthetic oviductal fluid (SOF), enriched
577 with 4 mg/mL BSA (Sigma A9647), non-essential and essential amino acids (SOFaa),
578 5 µg/mL insulin, 5 µg/mL transferrin, and 5 ng/mL selenium. The droplets were covered
579 with 900 µL paraffin oil (SAGE oil for tissue culture, ART-4008-5P, Cooper Surgical
580 Company). *In vitro* culture was performed at 38.5 °C in 5% CO_2, 5% O_2, and 90% N_2.

581 *Blastomere dissociation and culture*

582 The presumptive zygotes were monitored from 26 to 36 hours post-fertilization (hpf)
583 every 30 minutes to identify a direct cleavage of the zygote into three or four
584 blastomeres (multipolar division) or into two blastomeres (bipolar division).
585 Blastomeres from embryos that cleaved into more than four cells or presented multiple
586 fragments were not processed further. Immediately upon the first division, embryos
587 were washed in Hepes-TALP and treated with 0.1% pronase (protease from *S. griseus*)
588 in TCM-199 to dissolve the *zona pellucida*. Next, the embryos were washed in TCM-
589 199 with 10% FBS and then transferred to Ca^{+2}/Mg^{+2}-free PBS with 0.05% BSA to
590 enhance blastomere dissociation, which was performed using a STRIPPER pipet
591 holder and 170 µm and 135 µm capillaries (Origio, Cooper Surgical, CT, US) in
592 Ca^{+2}/Mg^{+2}-free PBS supplemented with 0.1% polyvinylpyrrolidone (PVP).
593 Subsequently, single blastomeres were washed in culture medium and transferred
594 individually to one well of a Primo VisionTM micro well group culture dish (Vitrolife,
595 Göteborg, Sweden), which contained a total of 16 small wells covered by a 40 µL
596 droplet of culture medium and 3.5 mL paraffin oil. Single blastomeres were cultured at
597 38.5°C in 5% CO_2, 5% O_2, and 90% N_2 until 72, 121 or 170 hpf according to the

experimental design.

Single-cell isolation

For isolation of single cells at 72 hpf, 121 hpf or from blastomeres that did not reach the blastocyst stage at 170 hpf, the outgrowths were transferred to Ca^{+2}/Mg^{+2}-free PBS with 0.1% PVP, and the cells were dissociated mechanically with a STRIPPER pipet holder and 170 µm and 135 µm capillaries (Origio, Cooper Surgical, CT, US). For blastomeres that reached the blastocyst stage at 170 hpf, single-cell isolation was done by incubating the embryos in trypsine-EDTA at 38.5°C, followed by washing in Ca^{+2}/Mg^{+2}-free PBS with 0.1% PVP, pipetting with a STRIPPER pipet holder, and 135 µm and 70 µm capillaries (Origio, Cooper Surgical, CT, US) and micromanipulation with holding (MPH-MED-35, Origio, Cooper Surgical, CT, US) and biopsy (MBB-BP-M-30, Origio, Cooper Surgical, CT, US) pipettes. When single-cell dissociation was not possible, clusters of cells were collected. Single cells from all time points were washed in Ca^{+2}/Mg^{+2}-free PBS with 0.1% PVP before transferring them into a well of a skirted 96-well plate (4ti-0960/C, AZENTA Life Sciences, Bioké, Leiden, The Netherlands) containing 2.5 µL of RLT lysis buffer with a 70 µm capillary (Origio, Cooper Surgical, CT, US) and a STRIPPER pipet holder screwed on 0.5 µL. The collected samples were kept on ice during the whole procedure and then stored at −80°C.

DNA and RNA separation, library preparation and sequencing

Separation of DNA and RNA from single cells

619 The DNA and mRNA from single cells were separated following the genome and
620 transcriptome sequencing (G&T-seq) protocol(Macaulay et al. 2016) on a robotic
621 liquid-handling platform (Microlab STAR Plus, Hamilton). Specifically, the 96-well
622 sample plate was positioned on the robot deck alongside (a) a plate for capturing poly-
623 A mRNAs, containing 10µl per well of Dynabeads® MyOneTM Streptavidin C1 (Thermo
624 Fisher Scientific) bound to biotinylated poly-dT oligos containing the SmartSeq2 primer
625 sequence '5BioTinTEG/ -
626 AAGCAGTGGTATCAACGCAGAGTACTTTTTTTTTTTTTTTTTTTTTTTTTTTTTTVN'
627 (IDT), (b) a plate for washing away DNA from the cell lysate supernatant, containing
628 25µl per well of G&T-wash buffer, and (c) an empty DNA destination plate. First, the
629 cell lysate was mixed with biotinylated poly-dT beads and incubated for 20 min.
630 Subsequently, beads bound to mRNA were pulled down using a low elution magnet
631 (Alpaqua) for 2 min, and the supernatant was transferred to the DNA destination plate.
632 Following this, the beads were subjected to two washes, each with 10µl of G&T wash
633 buffer, and the supernatant was transferred to the DNA destination plate. The DNA
634 destination plate, containing 37.5µl of G&T wash buffer, was then centrifuged for 1 min
635 at 1000g and stored at -80°C.

636 *RNA amplification, library preparation and sequencing*

637 The plate containing poly-A mRNA-bound beads was processed using an adapted
638 SmartSeq2 protocol with 20 PCR cycles. Subsequently, the amplified single-cell cDNA
639 was purified using a 0.8:1 ratio of Agencourt AMPure XP beads (Analis), followed by
640 washing with 80% ethanol and elution in water. Libraries were generated from the

641 amplified cDNA according to the Nextera XT (Illumina) protocol with quarter volumes.
642 These libraries were pooled and sequenced using single-end 50 sequencing on a
643 HiSeq4000 Illumina sequencer, aiming at 1 million reads per sample. For a subset of
644 blastocyst stage single cells, the libraries were resequenced paired-end 150 on a
645 NovaSeq 6000 Illumina sequencer for more reads.

646 *DNA amplification, GBS library preparation and sequencing*

647 For each blastomere outgrowth, DNA from either individual single cell or several cells
648 was used for GBS (with double enzyme restriction) processing. A sibling blastocyst
649 was collected and processed together when available. Whole-genome amplification
650 (WGA) was carried out using the REPLI-g SC kit (Qiagen, Germany) following the
651 manufacturer's guidelines, with variations in reaction volumes (full or half) and an
652 incubation period of 2-3 hours. The DNA separated from the single cells stored in G&T
653 wash buffer (see before), was thawn on ice, centrifuged for 1 min at 1000g, purified
654 with Agencourt AMPure XP beads (Beckman Coulter, USA), eluted in 4 µl of scPBS
655 and processed following the REPLI-g SC kit (Qiagen, Germany) manufacturer's
656 guidelines with an incubation time of 2h. Additionally, bulk DNA was extracted from
657 ovarian tissue of the donor cows (mothers of the respective embryos), semen from the
658 bull (father of the embryos), and blood from the parents of the bull (paternal
659 grandparents of the embryos) using the DNeasy Blood and Tissue kit (Qiagen,
660 Germany).

661 The whole-genome amplified DNA and bulk DNA were subjected to double restriction

662 digestion with 8 units (U) of PstI-HF (R3140S, NEB) and 4U of CviAII (R0640L, NEB)
663 enzymes (New England Biolabs, NEB, USA) combined with adapter ligation using 200-
664 300 ng as an input DNA for each sample. The restriction-ligation reaction was
665 performed in a total reaction volume of 15 µl, with a final concentration of 1X rCutSmart
666 buffer (B6004S, NEB), 1mM ATP (P0756S, NEB) and 160U of T4 DNA Ligase (M0202L,
667 NEB). Next, the double-sided size-selection was performed with Agencourt AMPure
668 XP beads (Beckman Coulter, USA) and 7 cycles of PCR to amplify and barcode size-
669 selected adapter-ligated fragments using Q5 High-Fidelity 2X Master Mix (NEB) and
670 0.5 µM primer mix with the following program. Subsequently, the libraries were purified
671 with Agencourt AMPure XP beads (Beckman Coulter, CA, USA), equimolarly pooled
672 and sequenced paired-end 150 on NovaSeq 6000 Illumina sequencer, with a target of
673 20-30 million reads per sample.

674 **Data analysis**

675 *GBS data processing, haplotyping and aneuploidy profiling*

676 The raw reads were processed using fastp (v0.23.2)(Chen et al. 2018) to trim adaptor
677 sequences, filter out low-quality reads, remove UMI sequences and append them to
678 read names. Next, cutadapt (v 1.18)(Martin 2011) was applied to select reads that start
679 with the internal barcode and trim off the barcode. Reads were then mapped to bovine
680 reference genome bosTau9 (ARS-UCD1.2) using BWA-MEM (v0.7.17)(Li 2013). Next,
681 UMICollapse(Liu 2019) was used for collapsing duplicated reads with the same UMI,
682 while accounting for sequencing/PCR errors. Across all samples, we obtained a

683 median of 64 million mapped reads. After UMI deduplication, a median of 35 million
684 mapped reads were retained (**Supplemental Table S2**). Variant calling was performed
685 with freebayes (v 1.3.2)(Garrison and Marth 2012). Initially, variants were called for the
686 parents and phasing reference(s) (parental grandparents or a sibling blastocyst).
687 Subsequently, the identified variants were utilized as input to call variants for each
688 single/multi-cell sample. The called SNVs were converted into bi-allelic calls (e.g., AA,
689 AB, and BB) with B-allele frequency (BAF) values calculated based on allele-specific
690 depth of coverage using a custom R script. The genotype calls and BAFs were then
691 used as input for the siCHILD pipeline (details in the method paper(Zamani Esteki et
692 al. 2015)). In brief, siCHILD performs pedigree-based haplotyping analysis. The
693 parents were first phased using phasing reference(s). Subsequently, for specific
694 combinations of phased parental genotypes, corresponding SNP BAF values of the
695 sample of interest were retrieved and plotted on paternal and maternal haplarithms.
696 Genome-wide parental haplotype inheritance can then be inferred through visual
697 inspection of the genome-wide haplarithm plots.

698 In addition to haplotype information, the R package QDNAseq and custom scripts were
699 applied to BAM files post-deduplication for aneuploidy profiling with a fixed bin size of
700 100kb. To quantify the extent of aneuploidy, the percentage of aneuploid autosomal
701 regions was calculated for each sample. Specifically, bins with a segmentation logR
702 value within $log2(1/2)$) and $\log2(3/2)$ were classified as normal, while all other bins
703 were classified as abnormal. The percentage of aneuploid autosomal regions was
704 calculated by summing up the length of all abnormal bins and dividing it by the size of

705 all autosomes. Samples were categorized based on the percentage of aneuploid
706 autosomal regions: $\leq \%1$ as euploid, 1-5% as low-level aneuploidy, 5-10% as
707 medium-level aneuploidy, and >10% as high-level aneuploidy. To determine
708 chromosome X nullisomy status, the lengths of all bins on chromosome X with a
709 segmentation logR value ≤ -3 were aggregated. The fraction of the chromosome X
710 region exhibiting nullisomy was determined by dividing this sum by the size of
711 chromosome X. Samples with >95% nullisomy in the chromosome X region were
712 classified as chromosome X nullisomy.

713 The haplotype composition and aneuploidy status of each blastomere outgrowth were
714 determined using GBS results from a single-cell/multi-cell sample. A sample was
715 considered anuclear if >60% and >10% of the reads mapped to the mitochondrial
716 genome before and after UMI deduplication, respectively, with empty haplarithm and
717 copy number plots. To infer an outgrowth to be anuclear, each cell in the outgrowth
718 was individually checked and confirmed to be anuclear. To verify the presence of
719 mitochondrial genomes in inferred anuclear biopsies and ascertain their maternal
720 inheritance, we exclusively called variants on the mitochondrial genome across all
721 inferred anuclear biopsies using Freebayes (v1.3.2)(Garrison and Marth 2012) and
722 compared the called genotypes (**Supplemental Table S3**).

723 *Single-cell RNA sequencing data preprocessing*

724 The raw reads were processed with fastp (v0.23.2)(Chen et al. 2018) to trim adaptor
725 sequences and filter out low-quality reads. Subsequently, the reads were mapped to

726 the bovine reference genome bosTau9 (ARS-UCD1.2) using STAR aligner (v
727 2.7.3)(Dobin et al. 2013) with Ensembl annotations ARS-UCD1.2.105. Next, raw
728 counts per cell were obtained using HTSeq (v 0.9.1)(Anders et al. 2015). Cells with
729 fewer than 200,000 detected molecules or fewer than 2,000 expressed genes were
730 excluded from further analysis, resulting in 446 cells out of 677 passing these quality
731 control thresholds. The retained cells exhibited a median of 862,384 molecules and
732 7,272 genes detected per cell (**Supplemental Table S2**). Counts were then normalized
733 and scaled using R package Seurat (v5.0.1)(Hao et al. 2023).

734 *Cell clustering, cell type identification and trajectory analysis*

735 Cell clustering was performed based on the normalized and scaled transcriptome
736 profiles using UMAP implemented in Seurat (v5.0.1). Subsequently, we assigned
737 molecular cell stage labels to each cluster based on the expression of (a) known
738 marker genes for ICM and TF (e.g. FN1, KDM2B for ICM, GATA3 for trophectoderm,
739 etc.(Negrón-Pérez et al. 2017; Nagatomo et al. 2013)); (b) genes first expressed at 4-
740 cell stage (minor EGA) or 8-16 cell stage (major EGA) in bovine embryos (Graf et al.
741 2014). For trajectory analysis, we employed the R package Slingshot (v2.10.0) to infer
742 developmental trajectories based on transcriptome profiles.

743 *Regulon analysis*

744 Regulon analysis was performed on the transcriptome data using pySCENIC
745 (v0.12.1)(Van de Sande et al. 2020). First, for each motif in the public collection
746 (https://resources.aertslab.org/cistarget/motif_collections/), genes in the bovine

747 reference genome bosTau9 (ARS-UCD1.2) with orthologs in humans were prioritized.
748 This prioritization was determined by a scoring system that assessed the presence of
749 the motif within a 10kb window upstream and downstream of the transcription start site.
750 Consequently, a motif x gene matrix was generated. Next, this matrix served as input
751 alongside the raw count matrix to pySCENIC (v0.12.1) to detect active regulons.
752 pySCENIC was run ten separate times, and only regulons appearing two or more times
753 were retained. The final AUC matrix was constructed using the maximum AUC values
754 for each regulon among all runs in which they were present. The AUC heatmap was
755 created with AUC values scaled for each regulon. To rank the identified regulons
756 according to their specificity in each cell lineage, a regulon specificity score was
757 calculated using "calcRSS" function within R package SCENIC (v 1.3.1). To identify the
758 key regulons for each molecular stage, we considered only regulons where
759 corresponding TFs were expressed in more than 50% of the cells. From these, for
760 each stage, we selected the top 6 regulons with the most frequent TF expression
761 among those ranked in the top 20 for both activity and specificity.

762 *Differential expression and regulon analysis*

763 Differential expression analysis was performed by comparing
764 androgenetic/gynogenetic/polyploid cells to biparental diploid cells within each
765 molecular cell stage using the FindMarkers function in Seurat (v5.0.1), employing the
766 "MAST" method with a minimum percentage threshold of 0.5. Pseudotime values and
767 aneuploid status were incorporated as latent variables in the model. Genes were
768 considered differentially expressed if they met the criteria of an adjusted p-value < 0.05

769 and an absolute log2 fold change greater than 1. Differential regulon analysis was
770 performed between cells exhibiting WG abnormalities and biparental diploid cells
771 within each molecular cell stage by Wilcoxon ranked-sum test on the AUC values.
772 Regulons were considered to have significantly different activity if they demonstrated
773 an adjusted *p*-value < 0.05 and an absolute log2 fold change greater than 1. The
774 functions of the differentially expressed genes and regulons were curated through
775 manual online searches and literature reviews.

776 *Statistical analysis*

777 Categorical data were compared using the chi-squared test, with Fisher's exact test
778 applied when cell counts were too small. Pseudotime values were compared using the
779 t-test. Statistical significance was determined using a two-tailed approach with a
780 significance threshold of $p < 0.05$. All tests were conducted in R (v4.3.2).

781 **Data access**

782 The GBS and single-cell RNA sequencing data reported in this paper are available at
783 the European Nucleotide Archive (ENA) under project number PRJEB76932
784 (https://www.ebi.ac.uk/ena/browser/view/PRJEB76932).

785 **Competing interests**

786 T.V. and J.R.V. are co-inventors on licensed patents WO/2011/157846 (Methods for
787 haplotyping single cells), WO/2014/053664 (High-throughput genotyping by
788 sequencing low amounts of genetic material) and WO/2015/028576 (Haplotyping and
789 copy number typing using polymorphic variant allelic frequencies).

Acknowledgements

Funding was received from the Marie Skłodowska-Curie grant agreement No 813707 (MATER) and from the KU Leuven, C1-C14/22/125 to J.R.V. and T.V. T.L. and T.V. were supported by the Research Foundation Flanders (FWO: G0C6120N, G088621N and I001818N). Y.Z. was supported by the Marie Skłodowska-Curie grant agreement No 813707 (MATER). A.F. is supported by the European Union's Horizon 2020 research and innovation programme under the Marie Skłodowska-Curie grant agreement No 860960 and BOF22/ITN/036.

Author contributions

J.R.V., A.V.S., and K.S. conceptualized and designed the study. A.F. conducted embryo experiments, with assistance from T.D.C. and D.A.V., T.L. and T.V. performed G&T-seq. G.P. and T.J. conducted GBS processing and coordinated sequencing. Y.Z. conducted bioinformatics analysis. Y.Z., J.R.V., and O.T. interpreted the data. Y.Z., J.R.V. A.F. and A.K. wrote the manuscript. All co-authors reviewed and approved the manuscript.

References

Anders S, Pyl PT, Huber W. 2015. HTSeq—a Python framework to work with high-throughput sequencing data. *Bioinformatics* **31**: 166. /pmc/articles/PMC4287950/ (Accessed March 22, 2024).

Bakshi A, Iturra FE, Alamban A, Rosas-Salvans M, Dumont S, Aydogan MG. 2023. Cytoplasmic division cycles without the nucleus and mitotic CDK/cyclin complexes. *Cell* **186**: 4694-4709.e16. http://www.cell.com/article/S0092867423010310/fulltext (Accessed March 27, 2024).

Balaban B, Brison D, Calderón G, Catt J, Conaghan J, Cowan L, Ebner T, Gardner D, Hardarson T, Lundin K, et al. 2011. The Istanbul consensus workshop on embryo assessment: proceedings of an expert meeting. *Human Reproduction* **26**: 1270–1283.

https://dx.doi.org/10.1093/humrep/der037 (Accessed May 22, 2024).

Caroselli S, Figliuzzi M, Picchetta L, Cogo F, Zambon P, Pergher I, Girardi L, Patassini C, Poli M, Bakalova D, et al. 2023. Improved clinical utility of preimplantation genetic testing through the integration of ploidy and common pathogenic microdeletions analyses. *Human Reproduction* **38**: 762–775. https://dx.doi.org/10.1093/humrep/dead033 (Accessed July 4, 2024).

Chatzimeletiou K, Morrison EE, Prapas N, Prapas Y, Handyside AH. 2005. Spindle abnormalities in normally developing and arrested human preimplantation embryos in vitro identified by confocal laser scanning microscopy. *Human Reproduction* **20**: 672–682. https://dx.doi.org/10.1093/humrep/deh652 (Accessed May 21, 2024).

Chen S, Zhou Y, Chen Y, Gu J. 2018. fastp: an ultra-fast all-in-one FASTQ preprocessor. *Bioinformatics* **34**: i884–i890. https://dx.doi.org/10.1093/bioinformatics/bty560 (Accessed March 22, 2024).

Coonen E, Rubio C, Christopikou Di, DImitriadou E, Gontar J, Goossens V, Maurer M, Spinella F, Vermeulen N, De Rycke M. 2020. ESHRE PGT Consortium good practice recommendations for the detection of structural and numerical chromosomal aberrations. *Hum Reprod Open* **2020**: 1–20. https://dx.doi.org/10.1093/hropen/hoaa017 (Accessed May 22, 2024).

Daughtry BL, Rosenkrantz JL, Lazar NH, Fei SS, Redmayne N, Torkenczy KA, Adey A, Yan M, Gao L, Park B, et al. 2019. Single-cell sequencing of primate preimplantation embryos reveals chromosome elimination via cellular fragmentation and blastomere exclusion. *Genome Res* **29**: 367–382. https://genome.cshlp.org/content/29/3/367.full (Accessed March 27, 2024).

De Coster T, Masset H, Tšuiko O, Catteeuw M, Zhao Y, Dierckxsens N, Aparicio AL, Dimitriadou E, Debrock S, Peeraer K, et al. 2022. Parental genomes segregate into distinct blastomeres during multipolar zygotic divisions leading to mixoploid and chimeric blastocysts. *Genome Biology 2022 23:1* **23**: 1–29. https://genomebiology.biomedcentral.com/articles/10.1186/s13059-022-02763-2 (Accessed March 27, 2024).

Deng Q, Huang S. 2004. PRDM5 is silenced in human cancers and has growth suppressive activities. *Oncogene 2004 23:28* **23**: 4903–4910. https://www.nature.com/articles/1207615 (Accessed June 21, 2024).

Destouni A, Esteki MZ, Catteeuw M, Tšuiko O, Dimitriadou E, Smits K, Kurg A, Salumets A, Van Soom A, Voet T, et al. 2016. Zygotes segregate entire parental genomes in distinct blastomere lineages causing cleavage-stage chimerism and mixoploidy. *Genome Res* **26**: 567–578. https://genome.cshlp.org/content/26/5/567.full (Accessed March 28, 2024).

Dobin A, Davis CA, Schlesinger F, Drenkow J, Zaleski C, Jha S, Batut P, Chaisson M, Gingeras TR. 2013. STAR: ultrafast universal RNA-seq aligner. *Bioinformatics* **29**: 15–21. https://pubmed.ncbi.nlm.nih.gov/23104886/ (Accessed March 22, 2024).

Dunn HO, McEntee K, Hansel W. 1970. Diploid-triploid chimerism in a bovine true hermaphrodite. *Cytogenet Genome Res* **9**: 245–259. https://dx.doi.org/10.1159/000130095 (Accessed March 28, 2024).

Fernandez Gallardo E, Sifrim A, Chappell J, Demeulemeester J, Herrmann JC, Vermotte R, Kerremans A, Van Der Haegen M, Herck J Van, Vanuytven S, et al. 2023. A multi-omics genome-and-transcriptome single-cell atlas of human preimplantation embryogenesis reveals the cellular and molecular impact of chromosome instability. *bioRxiv* 2023.03.08.530586. https://www.biorxiv.org/content/10.1101/2023.03.08.530586v1 (Accessed March 21, 2024).

Fragouli E, Alfarawati S, Spath K, Jaroudi S, Sarasa J, Enciso M, Wells D. 2013. The origin and impact of embryonic aneuploidy. *Hum Genet* **132**: 1001–1013. https://link.springer.com/article/10.1007/s00439-013-1309-0 (Accessed April 19, 2024).

Garrison E, Marth G. 2012. Haplotype-based variant detection from short-read sequencing. https://arxiv.org/abs/1207.3907v2 (Accessed March 22, 2024).

Gerri C, McCarthy A, Alanis-Lobato G, Demtschenko A, Bruneau A, Loubersac S, Fogarty NME, Hampshire D, Elder K, Snell P, et al. 2020. Initiation of a conserved trophectoderm program in human, cow and mouse embryos. *Nature 2020 587:7834* **587**: 443–447. https://www.nature.com/articles/s41586-020-2759-x (Accessed March 21, 2024).

Graf A, Krebs S, Zakhartchenko V, Schwalb B, Blum H, Wolf E. 2014. Fine mapping of genome activation in bovine embryos by RNA sequencing. *Proc Natl Acad Sci U S A* **111**: 4139–4144. https://pubmed.ncbi.nlm.nih.gov/24591639/ (Accessed March 22, 2024).

Hansen PJ. 2010. Medawar redux - an overview on the use of farm animal models to elucidate principles of reproductive immunology. *Am J Reprod Immunol* **64**: 225–230. https://pubmed.ncbi.nlm.nih.gov/20678170/ (Accessed June 21, 2024).

Hao Y, Lai L, Mao J, Im GS, Bonk A, Prather RS. 2004. Apoptosis in Parthenogenetic Preimplantation Porcine Embryos. *Biol Reprod* **70**: 1644–1649. https://dx.doi.org/10.1095/biolreprod.103.026005 (Accessed May 21, 2024).

Hao Y, Stuart T, Kowalski MH, Choudhary S, Hoffman P, Hartman A, Srivastava A, Molla G, Madad S, Fernandez-Granda C, et al. 2023. Dictionary learning for integrative, multimodal and scalable single-cell analysis. *Nature Biotechnology 2023 42:2* **42**: 293–304. https://www.nature.com/articles/s41587-023-01767-y (Accessed March 22, 2024).

Hardy K, Handyside AH, Winston RML. 1989. The human blastocyst: cell number, death and allocation during late preimplantation development in vitro. *Development* **107**: 597–604. https://dx.doi.org/10.1242/dev.107.3.597 (Accessed March 28, 2024).

Hardy K, Winston RML, Handyside AH. 1993. Binucleate blastomeres in preimplantation human embryos in vitro: failure of cytokinesis during early cleavage. *Reproduction* **98**: 549–558. https://rep.bioscientifica.com/view/journals/rep/98/2/jrf_98_2_032.xml (Accessed May 21, 2024).

Hassold T, Chen N, Funkhouser J, Jooss T, Manuel B, Matsuura J, Matsuyama A, Wilson C, Yamane JA, Jacobs PA. 1980. A cytogenetic study of 1000 spontaneous abortions. *Ann Hum Genet* **44**: 151–164. https://onlinelibrary.wiley.com/doi/full/10.1111/j.1469-1809.1980.tb00955.x (Accessed May 15, 2024).

Hassold T, Hunt P. 2001. To err (meiotically) is human: the genesis of human aneuploidy. *Nature Reviews Genetics 2001 2:4* **2**: 280–291. https://www.nature.com/articles/35066065 (Accessed April 23, 2024).

Home P, Kumar RP, Ganguly A, Saha B, Milano-Foster J, Bhattacharya B, Ray S, Gunewardena S, Paul A, Camper SA, et al. 2017. Genetic redundancy of GATA factors in the extraembryonic trophoblast lineage ensures the progression of preimplantation and postimplantation mammalian development. *Development (Cambridge)* **144**: 876–888. https://dx.doi.org/10.1242/dev.145318 (Accessed March 21, 2024).

Hoppe PC, Illmensee K. 1977. Microsurgically produced homozygous-diploid uniparental mice. *Proceedings of the National Academy of Sciences* **74**: 5657–5661. https://www.pnas.org/doi/abs/10.1073/pnas.74.12.5657 (Accessed May 21, 2024).

Hwang IS, Park MR, Lee HS, Kwak TU, Son HY, Kang JK, Lee JW, Lee K, Park EW, Hwang S. 2020. Developmental and Degenerative Characterization of Porcine Parthenogenetic Fetuses during Early Pregnancy. *Animals 2020, Vol 10, Page 622* **10**: 622. https://www.mdpi.com/2076-2615/10/4/622/htm (Accessed May 21, 2024).

Ito M, Kaneko-Ishino T, Ishino F, Matsuhashi M, Yokoyama M, Katsuki M. 1991. Fate of haploid parthenogenetic cells in mouse chimeras during development. *Journal of Experimental Zoology* **257**: 178–183. https://onlinelibrary.wiley.com/doi/full/10.1002/jez.1402570206 (Accessed May 21, 2024).

Johnson WH, Loskutoff NM, Plante Y, Betteridge KJ. 1995. Production of four identical calves by the separation of blastomeres from an in vitro derived four-cell embryo. *Vet Rec* **137**: 15–16. https://europepmc.org/article/med/7483226 (Accessed March 28, 2024).

Kola I, Trounson A, Dawson G, Rogers P. 1987. Tripronuclear human oocytes: altered cleavage

patterns and subsequent karyotypic analysis of embryos. *Biol Reprod* **37**: 395–401. https://pubmed.ncbi.nlm.nih.gov/3676394/ (Accessed April 22, 2024).

Leng L, Ouyang Q, Kong X, Gong F, Lu C, Zhao L, Shi Y, Cheng D, Hu L, Lu G, et al. 2017. Self-diploidization of human haploid parthenogenetic embryos through the Rho pathway regulates endomitosis and failed cytokinesis. *Scientific Reports 2017 7:1* **7**: 1–10. https://www.nature.com/articles/s41598-017-04602-y (Accessed May 22, 2024).

Leng L, Sun J, Huang J, Gong F, Yang L, Zhang S, Yuan X, Fang F, Xu X, Luo Y, et al. 2019. Single-Cell Transcriptome Analysis of Uniparental Embryos Reveals Parent-of-Origin Effects on Human Preimplantation Development. *Cell Stem Cell* **25**: 697-712.e6. http://www.cell.com/article/S1934590919303893/fulltext (Accessed March 28, 2024).

Li H. 2013. Aligning sequence reads, clone sequences and assembly contigs with BWA-MEM. *arXiv: Genomics*.

Liu D. 2019. Algorithms for efficiently collapsing reads with Unique Molecular Identifiers. *PeerJ* **7**. /pmc/articles/PMC6921982/ (Accessed March 22, 2024).

Liu L, Trimarchi JR, Keefe DL. 2002. Haploidy but Not Parthenogenetic Activation Leads to Increased Incidence of Apoptosis in Mouse Embryos. *Biol Reprod* **66**: 204–210. https://dx.doi.org/10.1095/biolreprod66.1.204 (Accessed May 21, 2024).

López-Maury L, Marguerat S, Bähler J. 2008. Tuning gene expression to changing environments: from rapid responses to evolutionary adaptation. *Nature Reviews Genetics 2008 9:8* **9**: 583–593. https://www.nature.com/articles/nrg2398 (Accessed July 1, 2024).

Lucifero D, Suzuki J, Bordignon V, Martel J, Vigneault C, Therrien J, Filion F, Smith LC, Trasler JM. 2006. Bovine SNRPN Methylation Imprint in Oocytes and Day 17 In Vitro-Produced and Somatic Cell Nuclear Transfer Embryos. *Biol Reprod* **75**: 531–538. https://dx.doi.org/10.1095/biolreprod.106.051722 (Accessed May 19, 2024).

Ma LB, Yang L, Zhang Y, Cao JW, Hua S, Li JX. 2008. Quantitative analysis of mitochondrial RNA in goat–sheep cloned embryos. *Mol Reprod Dev* **75**: 33–39. https://onlinelibrary.wiley.com/doi/full/10.1002/mrd.20736 (Accessed March 27, 2024).

Macaulay IC, Teng MJ, Haerty W, Kumar P, Ponting CP, Voet T. 2016. Separation and parallel sequencing of the genomes and transcriptomes of single cells using G&T-seq. *Nature Protocols 2016 11:11* **11**: 2081–2103. https://www.nature.com/articles/nprot.2016.138 (Accessed March 22, 2024).

Madan K. 2020. Natural human chimeras: A review. *Eur J Med Genet* **63**: 103971.

Marsico TV, Valente RS, Annes K, Oliveira AM, Silva MV, Sudano MJ. 2023. Species-specific

molecular differentiation of embryonic inner cell mass and trophectoderm: A systematic review. *Anim Reprod Sci* **252**: 107229.

Martin M. 2011. Cutadapt removes adapter sequences from high-throughput sequencing reads. *EMBnet J* **17**: 10–12. https://journal.embnet.org/index.php/embnetjournal/article/view/200/479 (Accessed March 22, 2024).

Masset H, Ding J, Dimitriadou E, Debrock S, Tšuiko O, Smits K, Peeraer K, Voet T, Esteki MZ, Vermeesch JR. 2022. Single-cell genome-wide concurrent haplotyping and copy-number profiling through genotyping-by-sequencing. *Nucleic Acids Res* **50**: e63–e63. https://dx.doi.org/10.1093/nar/gkac134 (Accessed May 23, 2024).

Masset H, Tšuiko O, Vermeesch JR. 2021. Genome-wide abnormalities in embryos: Origins and clinical consequences. *Prenat Diagn* **41**: 554–563.

May-Panloup P, Vignon X, Chrétien MF, Heyman Y, Tamassia M, Mathièry Y, Reynier P. 2005. Increase of mitochondrial DNA content and transcripts in early bovine embryogenesis associated with upregulation of mtTFA and NRF1 transcription factors. *Reproductive Biology and Endocrinology* **3**: 1–8. https://rbej.biomedcentral.com/articles/10.1186/1477-7827-3-65 (Accessed March 27, 2024).

McCoy RC, Demko ZP, Ryan A, Banjevic M, Hill M, Sigurjonsson S, Rabinowitz M, Petrov DA. 2015. Evidence of Selection against Complex Mitotic-Origin Aneuploidy during Preimplantation Development. *PLoS Genet* **11**. https://www.notion.so (Accessed May 21, 2024).

Meinecke B, Kuiper H, Drögemüller C, Leeb T, Meinecke-Tillman S. 2003. A Mola Hydatidosa Coexistent with a Foetus in a Bovine Freemartin Pregnancy. *Placenta* **24**: 107–112.

Nagatomo H, Kagawa S, Kishi Y, Takuma T, Sada A, Yamanaka K ichi, Abe Y, Wada Y, Takahashi M, Kono T, et al. 2013. Transcriptional Wiring for Establishing Cell Lineage Specification at the Blastocyst Stage in Cattle1. *Biol Reprod* **88**: 158–159. https://dx.doi.org/10.1095/biolreprod.113.108993 (Accessed March 21, 2024).

Negrón-Pérez VM, Zhang Y, Hansen PJ. 2017. Single-cell gene expression of the bovine blastocyst. *Reproduction* **154**: 627–644. https://rep.bioscientifica.com/view/journals/rep/154/5/REP-17-0345.xml (Accessed March 21, 2024).

Niakan KK, Eggan K. 2013. Analysis of human embryos from zygote to blastocyst reveals distinct gene expression patterns relative to the mouse. *Dev Biol* **375**: 54–64.

Ottolini CS, Kitchen J, Xanthopoulou L, Gordon T, Summers MC, Handyside AH. 2017. Tripolar

mitosis and partitioning of the genome arrests human preimplantation development in vitro. *Scientific Reports 2017 7:1* **7**: 1–10. https://www.nature.com/articles/s41598-017-09693-1 (Accessed March 28, 2024).

Santos RR, Schoevers EJ, Roelen BAJ. 2014. Usefulness of bovine and porcine IVM/IVF models for reproductive toxicology. *Reprod Biol Endocrinol* **12**: 1–12. https://pubmed.ncbi.nlm.nih.gov/25427762/ (Accessed June 21, 2024).

Seckl MJ, Sebire NJ, Berkowitz RS. 2010. Gestational trophoblastic disease. *The Lancet* **376**: 717–729.

Sherard J, Bean C, Bove B, DelDuca V, Esterly KL, Karcsh HJ, Munshi G, Reamer JF, Suazo G, Wilmoth D. 1986. Long survival in a 69,XXY triploid male. *Am J Med Genet* **25**: 307–312. https://pubmed.ncbi.nlm.nih.gov/3777027/ (Accessed May 15, 2024).

Shu X sheng, Geng H, Li L, Ying J, Ma C, Wang Y, Poon FF, Wang X, Ying Y, Yeo W, et al. 2011. The Epigenetic Modifier PRDM5 Functions as a Tumor Suppressor through Modulating WNT/β-Catenin Signaling and Is Frequently Silenced in Multiple Tumors. *PLoS One* **6**: e27346. https://journals.plos.org/plosone/article?id=10.1371/journal.pone.0027346 (Accessed June 21, 2024).

Sigalos G, Triantafyllidou O, Vlahos NF. 2016. Novel embryo selection techniques to increase embryo implantation in IVF attempts. *Arch Gynecol Obstet* **294**: 1117–1124. https://link.springer.com/article/10.1007/s00404-016-4196-5 (Accessed May 22, 2024).

Sugimura S, Akai T, Hashiyada Y, Somfai T, Inaba Y, Hirayama M, Yamanouchi T, Matsuda H, Kobayashi S, Aikawa Y, et al. 2012. Promising System for Selecting Healthy In Vitro–Fertilized Embryos in Cattle. *PLoS One* **7**: e36627. https://journals.plos.org/plosone/article?id=10.1371/journal.pone.0036627 (Accessed March 26, 2024).

Sugimura S, Akai T, Imai K. 2017. Selection of viable in vitro-fertilized bovine embryos using time-lapse monitoring in microwell culture dishes. *Journal of Reproduction and Development* **63**: 353–357.

Tarkowski AK. 1977. In vitro development of haploid mouse embryos produced by bisection of one-cell fertilized eggs. *Development* **38**: 187–202. https://dx.doi.org/10.1242/dev.38.1.187 (Accessed May 21, 2024).

Thundathil J, Filion F, Smith LC. 2005. Molecular control of mitochondrial function in preimplantation mouse embryos. *Mol Reprod Dev* **71**: 405–413. https://onlinelibrary.wiley.com/doi/full/10.1002/mrd.20260 (Accessed March 27, 2024).

Tšuiko O, Catteeuw M, Esteki MZ, Destouni A, Pascottini OB, Besenfelder U, Havlicek V, Smits

K, Kurg A, Salumets A, et al. 2017. Genome stability of bovine in vivo-conceived cleavage-stage embryos is higher compared to in vitro-produced embryos. *Human Reproduction* **32**: 2348–2357. https://dx.doi.org/10.1093/humrep/dex286 (Accessed March 28, 2024).

Tšuiko O, Vanneste M, Melotte C, Ding J, Debrock S, Masset H, Peters M, Salumets A, De Leener A, Pirard C, et al. 2021. Haplotyping-based preimplantation genetic testing reveals parent-of-origin specific mechanisms of aneuploidy formation. *NPJ Genom Med* **6**. /pmc/articles/PMC8497526/ (Accessed May 29, 2024).

Van de Sande B, Flerin C, Davie K, De Waegeneer M, Hulselmans G, Aibar S, Seurinck R, Saelens W, Cannoodt R, Rouchon Q, et al. 2020. A scalable SCENIC workflow for single-cell gene regulatory network analysis. *Nature Protocols 2020 15:7* **15**: 2247–2276. https://www.nature.com/articles/s41596-020-0336-2 (Accessed March 22, 2024).

Vanneste E, Voet T, Le Caignec C, Ampe M, Konings P, Melotte C, Debrock S, Amyere M, Vikkula M, Schuit F, et al. 2009. Chromosome instability is common in human cleavage-stage embryos. *Nature Medicine 2009 15:5* **15**: 577–583. https://www.nature.com/articles/nm.1924 (Accessed March 28, 2024).

Willadsen SM. 1980. The viability of early cleavage stages containing half the normal number of blastomeres in the sheep. *Reproduction* **59**: 357–362. https://rep.bioscientifica.com/view/journals/rep/59/2/jrf_59_2_015.xml (Accessed March 28, 2024).

Wydooghe E, Vaele L, Piepers S, Dewulf J, Van Abbeel E Den, De Sutter P, Van Soom A. 2014. Individual commitment to a group effect: strengths and weaknesses of bovine embryo group culture. *Reproduction* **148**: 519–529. https://pubmed.ncbi.nlm.nih.gov/25118302/ (Accessed April 22, 2024).

Xu J, Shu Y, Yao G, Zhang Y, Niu W, Zhang Y, Ma X, Jin H, Zhang F, Shi S, et al. 2021. Parental methylome reprogramming in human uniparental blastocysts reveals germline memory transition. *Genome Res* **31**: 1519. /pmc/articles/PMC8415376/ (Accessed May 21, 2024).

Zamani Esteki M, Dimitriadou E, Mateiu L, Melotte C, Van der Aa N, Kumar P, Das R, Theunis K, Cheng J, Legius E, et al. 2015. Concurrent Whole-Genome Haplotyping and Copy-Number Profiling of Single Cells. *Am J Hum Genet* **96**: 894. /pmc/articles/PMC4473724/ (Accessed March 22, 2024).

Zaragoza M V., Surti U, Redline RW, Millie E, Chakravarti A, Hassold TJ. 2000. Parental origin and phenotype of triploidy in spontaneous abortions: Predominance of diandry and association with the partial hydatidiform mole. *Am J Hum Genet* **66**: 1807–1820. http://www.cell.com/article/S0002929707635332/fulltext (Accessed March 4, 2024).

Zhan Q, Ye Z, Clarke R, Rosenwaks Z, Zaninovic N. 2016. Direct Unequal Cleavages: Embryo

Developmental Competence, Genetic Constitution and Clinical Outcome. *PLoS One* **11**: e0166398. https://journals.plos.org/plosone/article?id=10.1371/journal.pone.0166398 (Accessed April 22, 2024).